the very different (by 0.116 Å) C-O bond lengths on one of the CH_3CO_2 fragments whereas the C-O bond lengths on the other fragment differ by only 0.026 Å. A similar comparison of C-C-O angles shows them to be very different in the assigned acid monomer and similar in the identified acetate anion fragment. It should be remembered that the $KH(CF_3CO_2)_2$ crystal has the symmetric (C_{2h}) syn-syn conformation[19] and that $KH(CH_3CO_2)_2$ has the asymmetric *syn*-acetic acid-*anti*-acetate anion conformation.[30] Thus, both the specific conformation and the number of minima in the proton energy profile in these dicarboxylic anions are strongly dependent on molecular structure and environmental effects.

The progression from structure **1** to **7** (Figure 3) shows some interesting geometrical and electronic structure features. In line with the previous discussion the H2···O8 distance (ρ) decreases, along with the combined C1—O4···H5 and H5···O6—C7 angles, which makes the decrease of ρ possible, as the larger charges on H2 and O8 develop. The calculated charge on the transferring proton actually stays constant at +0.31 within ±0.02 units from the initial (**1**) to the final (**7**) complex, without ever developing the expected near full charge of +1.00. This results corresponds to the charge relay model of H bonding discussed by Zuccarello and Del Re.[33]

Summary

Two symmetric [C_{2h}(I), C_{2h}(II)] and two asymmetric (anti, syn) formic acid-formate anion dimer structures have been determined. The calculated (SCF,MP2) binding energy values are the following: anti (28.8, 33.0) > C_{2h}(I) (24.7, ~32) > syn (23.2, 28.9) ≈ C_{2h}(II) (21.7, 29.2), in kcal/mol. The anti conformer is identified with the biformate anion for which a gas-phase binding energy of 36.8 kcal/mol has been measured by Meot-Ner and Sieck.[19] The other calculated structures, as well as additional conformer types, are found experimentally in crystal structures of bicarboxylic acids. Comparison of bond lengths and angles between calculated and observed crystal structures for the corresponding conformations shows very good agreement. The calculated stability of the anti dimer includes a C—H···O interaction which is estimated to contribute approximately 2.4 (SCF) or 1.8 (MP2) kcal/mol to the dimer energy. The greater stability of the anti dimer relative to the syn conformer can be attributed both to less interfragment exchange repulsion and to more coulomb attraction in the former structure.

The optimized proton transfer curve connecting the two asymmetric dimers as a function of one O-H distance shows a (syn dimer) inflection point and an (anti dimer) minimum, while the MP2 curve shows only a single (anti dimer) minimum. However, the proton transfer energy profiles for a series of fixed R(O···O) distances in the strong H-bond region each show two minima, with the anti dimer always lower in energy, except at R_{min} where the minima merge.

The existence of all these conformer combinations experimentally and the small energy differences calculated between them theoretically shows the sensitivity of the specific conformation of this strong H-bond system to molecular structure, environment, and level of theoretical treatment.

(33) Zuccarello, F.; Del Re, G. *J. Compt. Chem.* **1987**, *8*, 816.

Second-Moment Equality and the Structural Chemistry of the Main-Group Intermetallic Compounds

Stephen Lee

Contribution from the Department of Chemistry, The University of Michigan, Ann Arbor, Michigan 48109-1055. *Received June 18, 1990*

Abstract: We determine electron counting rules for $ZA_{2-x}B_x$ compounds, where Z is an electropositive atom and A and B are main-group atoms. These rules are derived from a Hückel-type theory. Agreement between theory and experiment for all the major $ZA_{2-x}B_x$ families, which include the $MgCu_2$, $MoSi_2$, $CeCd_2$, $CeCu_2$, MgAgAs, $CaIn_2$, AlB_2, $ThSi_2$, and Cu_2Sb structure types, is excellent. The results are interpreted by use of the method of moments.

Introduction

In recent years, research done by several groups has shown that tight-binding band calculations can provide useful insight to the structural preferences of solid-state compounds.[1] General application of the method, however, has generally been hampered by problems related to coordination number.[2] For example, the two forms of carbon, diamond and graphite, are known to have rather similar electronic energies. However, a tight-binding or Hückel calculation on the two structures based on the observed experimental densities shows that diamond is lower in energy by 1 eV/atom. The problem is that diamond contains four-coordinate carbon while graphite contains three-coordinate carbon. As the tight-binding method ignores electron-electron interaction, the higher coordinate geometry is typically the favored one. In this paper, we follow a novel method of removing this coordination number problem.

We demonstrate its utility by studying compounds with the stoichiometry $ZA_{2-x}B_x$, where Z is an electropositive element from the first four columns of the periodic table and A or B are elements from columns 8-16. There are 14 major families. They are the $MgZn_2$, $MgCu_2$, Cu_2Sb, $MoSi_2$, Fe_2P, Co_2Si, $CeCu_2$, MgAgAs, $CdCd_2$, $CaIn_2$, $InNi_2$, AlB_2, $ThSi_2$, and $ZrSi_2$ structure types.[3] (By major we mean structure types with at least two dozen known compounds.) In this paper, we will not discuss the $MgZn_2$, Fe_2P,

(1) (a) Pettifor, D. G. *J. Phys. Chem.* **1970**, *2*, 366. (b) Duthie, J.; Pettifor, D. G. *Phys. Rev. Lett.* **1977**, *38*, 564. (c) Hoffmann, R. *Solids and Surfaces: A Chemist's View of Bonding in Extended Structures*; VCH Publishers: New York, 1988. (d) Burdett, J. K. *Prog. Solid State Chem.* **1984**, *15*, 173. (e) Whangbo, M.-H. In *Crystal Chemistry and Properties of Materials with Quasi One Dimensional Structures*: Rouxel, J., Ed.; Reidel: Dordrecht, 1986, p 27.

(2) However, see: (a) Lee, S.; Hoistad, L. M. *J. Am. Chem. Soc.* **1990**, submitted for publication.

(3) (a) $MgZn_2$: Friauf, J. *Phys. Rev.* **1927**, *29*, 34. (b) $MgCu_2$: Grime, G.; Morris-Jones, W. *Philos. Mag.* **1929**, *7*, 1113. (c) Cu_2Sb: Elander, M.; Hägg, G.; Westgren, A. *Ark. Kemi Mineral. Geol.* **1935**, *12B*, 1. (d) $MoSi_2$: *Strukturbericht 1*, 740. (e) Fe_2P: Rundqvist, S.; Jellinek, F. *Acta. Chem. scand.* **1959**, *13*, 425. (f) Co_2Si: Geller, S. *Acta Crystallogr.* **1955**, *8*, 83. (g) $CeCu_2$: Larson, A. C. *Acta Crystallogr.* **1961**, *14*, 73. (h) $CeCd_2$: Iandelli, A.; Ferro, R. *Chim. Ital. Gazz.* **1954**, *84*, 463. (i) MgAgAs: Nowotny, H.; Sibert, W. *Z. Metallkd.* **1941**, *33*, 391. (j) $ThSi_2$: Brauer, G.; Mitius, A. *Z. Anorg. Allg. Chem.* **1942**, *345*, 249. (k) $ZrSi_2$: Vaughn, P. *Am. Crystallogr. Assoc. Summer Meeting* **1955**, 8. (l) Villars, P.; Calvert, L. D. *Pearson's Handbook of Crystallographic Data for Intermetallic Phases*; American Society of Metals: Metals Park, OH, 1985.

0002-7863/91/1513-101$02.50/0

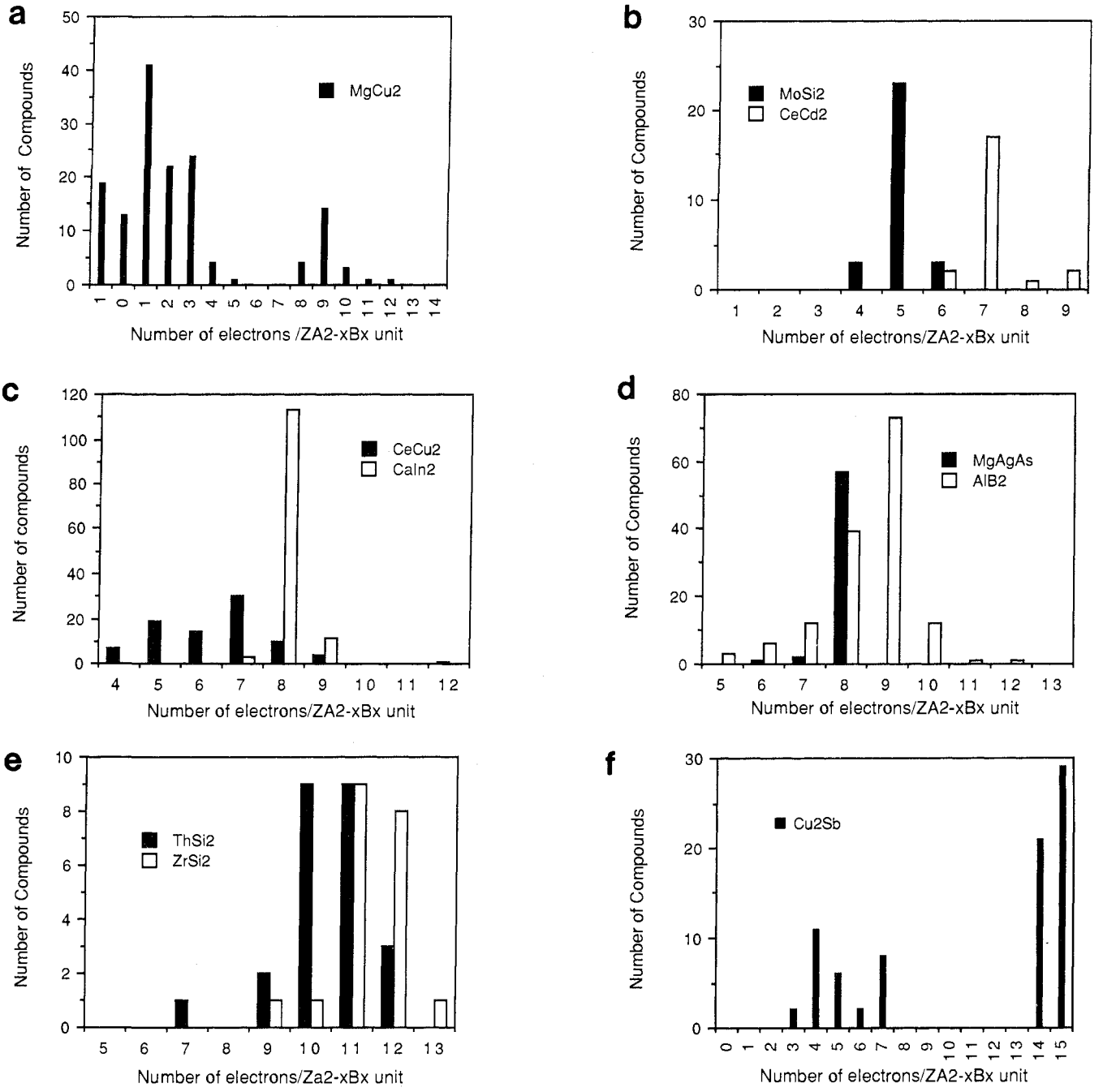

Figure 1. Number of compounds found for a given number of electrons for (a) the $MgCu_2$ st, (b) $MoSi_2$ and $CeCd_2$ st, (c) $CeCu_2$ and $CaIn_2$ st, (d) MgAgAs and AlB_2 st, (e) $ThSi_2$ and $ZrSi_2$ st, and (f) Cu_2Sb st. The abscissa shows the number of valence electrons per $ZA_{2-x}B_x$ unit. Electron counting was done by the procedure stated in ref 2. Data are taken from ref 31.

$InNi_2$, and Co_2Si structure types. The first has already been considered elsewhere,[4] and the latter three will be the subject of separate investigation.[5] In total in the remaining families, ref 31 lists over 750 separate compounds.

These structures have particular electron counts for which they are most often found. In some cases the structure type occurs at a rather precise electron count ($CaIn_2$ and $MoSi_2$), while in other cases the zones of stability are rather broad (AlB_2 and $CeCu_2$). In Figure 1, we plot in histogram form the electron counts for the experimentally known phases. It may be seen that the electron count provides some, but not complete, separation between the different structure types. (For a more complete separation, it is generally necessary to introduce a second variable.)[6] In Table I, we combine these histograms and show that at any one particular electron count only a few structure types are observed. Furthermore, in Table I we have italicized the most common electron count (the mode) for each of the 10 structure types. It may be seen that these modes may be placed in a sequence. Starting from one electron per $ZA_{2-x}B_x$ unit, we find the first mode is that of the $MgCu_2$ type. The remaining modes follow in the sequence: $MoSi_2$, $CeCd_2$ = $CeCu_2$, MgAgAs = $CaIn_2$, AlB_2, $ThSi_2$, $ZrSi_2$, and finally Cu_2Sb.

(4) The tight-binding method has been previously applied to the $MgZn_2$, $MgCu_2$, and $MgNi_2$ phases in: (a) Haydock, R.; Johannes, R. L. *J. Phys. F: Met. Phys.* **1975**, *5*, 2055. (b) Johannes, R. L.; Haydock, R.; Heine, V. *Phys. Rev. Lett.* **1976**, *36*, 372.

(5) We do not include the Fe_2P, Co_2Si, and $InNi_2$ phases here, as these compounds are practically always of ternary composition with one electropositive atom (Z), one transition-metal (A), and one main-group atom (B). To study these structure types, we therefore need to include the effect of having different A and B atoms in the ZAB phase.

(6) For a recent discussion of structure maps, see: Hafner, J. *From Hamiltonians to Phase Diagrams*; Springer-Verlag: Berlin, 1987; p 207.

Table I. Predicted and Observed Zones of Stability of $ZA_{2-x}B_x$

no. of electrons $ZA_{2-x}B_x$ unit	theory[a]	expt[b]
1	$MgCu_2$	*$MgCu_2$*
2	$MgCu_2$	$MgCu_2$
3	$MgCu_2$	$MgCu_2$
4	$MoSi_2$ = (Cu_2Sb) > $MgCu_2$ > $CeCd_2$	Cu_2Sb,$MgCu_2$
5	$MoSi_2$ = (Cu_2Sb)	*$MoSi_2$*, Cu_2Sb, $CeCu_2$
6	$MoSi_2$ = (Cu_2Sb) = $CeCd_2$ > $CeCu_2$	complex
7	$CeCd_2$ = $CeCu_2$ = MgAgAs = ($CaIn_2$)	*$CeCd_2$*, *$CeCu_2$*, Cu_2Sb, AlB_2
8	MgAgAs = ($CaIn_2$)	*MgAgAs*, *$CaIn_2$*
9	AlB_2 > $ThSi_2$	*AlB_2*, $MgCu_2$
10	$ThSi_2$ > AlB_2	*$ThSi_2$*
11	see text	*$ZrSi_2$*, *$ThSi_2$*
12	see text	$ZrSi_2$
13	$ZrSi_2$ = Cu_2Sb	$ZrSi_2$
14	Cu_2Sb	Cu_2Sb
15	Cu_2Sb	*Cu_2Sb*

[a] Parentheses indicate a structure for which no calculation has been carried out but which is geometrically similar to another structure type. Equality signs indicate the structure types are within 0.05 eV/atom of one another. Greater than signs indicate alternative structures that have energies within 0.40 eV/atom of the most stable structure. [b] Italicized compounds indicate the mode for that structure type.

The Crystal Structure

In Figure 2, we illustrate the structures of these 10 structure types. It may be seen that the structure types with neighboring electronic zones of stability share certain geometric features in common. The $MgCu_2$ structure contains triangles of bonded atoms. $MoSi_2$ contains both triangles and squares. $CeCd_2$ and $CeCu_2$ contain both squares and hexagons. AlB_2, $CaIn_2$, and MgAgAs contain only hexagons. $ThSi_2$ has no small rings. $ZrSi_2$ is composed of two nets. One has no small rings (it is a chain structure); the other is a square lattice. Electron-rich Cu_2Sb contains only squares and nonbonded atoms. The trend is therefore for low-electron-count phases to have structures with just triangles, at slightly less than the half-filled band to have structures with a complex assortment of rings, at the half-filled band to have hexagons, at slightly higher than the half-filled band to have open structures, and near the filled band to have squares alone.

This sequence is similar to a composite curve that was earlier described with the moment method.[7] The results of our earlier work are shown in Figure 3a. It should be noted, however, that the location of the nodes of the curves drawn in Figure 3a are subject to variation. This variation is primarily caused by the overall shape of the density of electronic states (DOS or ρ). For rather uniform DOS, Figure 3a is qualitatively correct. However, in the case of tails,[7,8] the nodes shift toward the direction of the tail. This is important. Triangles and especially tetrahedra create strong tails in the extreme bonding region of the DOS. In the presence of many triangles, the curve more correctly takes on the shape shown in Figure 3b. Therefore, it becomes possible for compounds that do not contain triangles to be stable at electron counts that are less than the half-filled band. Another defect in Figure 3a is the inclusion of the five-membered ring curve. Fivefold symmetry is forbidden in crystal structures, and hence,

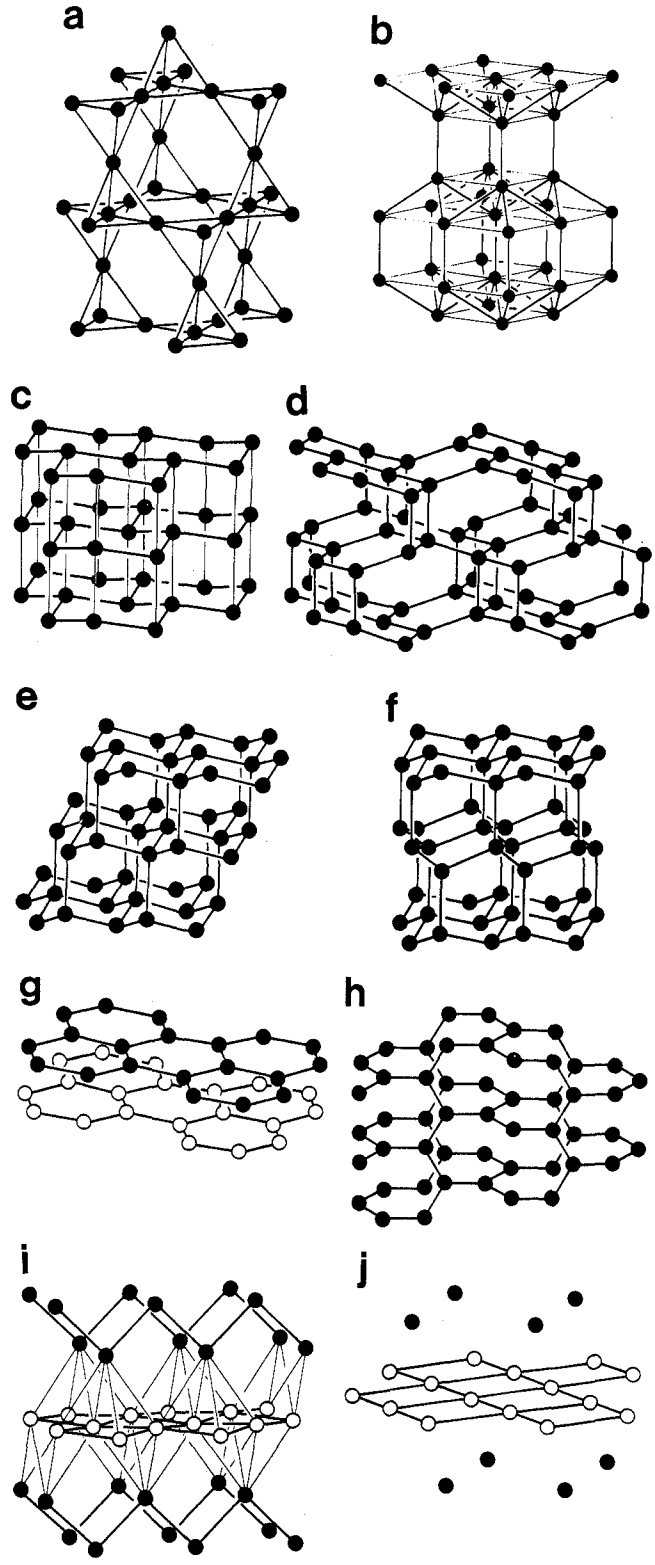

Figure 2. Covalent network found in the (a) $MgCu_2$ st, (b) $MoSi_2$ st, (c) $CeCd_2$ st, (d) $CeCu_2$ st, (e) MgAgAs st or diamond, (f) $CaIn_2$ st, (g) AlB_2 st, (h) $ThSi_2$ st, (i) $ZrSi_2$ st, and (j) electron-rich Cu_2Sb st. Thick lines correspond to the shorter interatomic distances listed in Table II. Thin lines (found for the $MoSi_2$, $CeCd_2$, and $ZrSi_2$ st) correspond to the larger interatomic distances listed in Table II.

(7) (a) Ducastelle, F.; Cyrot-Lackmann, F. *J. Phys. Chem. Solids* **1970**, *31*, 1295. (b) Burdett, J. K.; Lee, S. *J. Am. Chem. Soc.* **1985**, *107*, 3050, 3063, 3083.

(8) Lee, S. *J. Am. Chem. Soc.* **1988**, *110*, 8000.

(9) (a) $GdAu_2$: McMasters, O. D.; Gschneider, K. A. Jr.; Bruzzone, G.; Palenzona, A. *J. Less-Common Met.* **1971**, *25*, 137. (b) $NaAu_2$: Perlitz, H.; Aruja, E. *Naturwiss* **1937**, *25*, 61. (c) $NdGe_2$: Gladyshevskii, E. T. *J. Struct. Chem. (Engl. Transl.)* **1964**, *5*, 523. (d) $PrGa_2$: Yatsenko, S. P.; Semyannikov, A. A.; Semenov, B. G.; Chuntonov, K. A. *J. Less-Common Met.* **1979**, *64*, 185. (e) $ZrGe_2$: Smith, J. F.; Bailey, D. M. *Acta Crystallogr.* **1957**, *10*, 341. (f) $YbSb_2$: Wang, R.; Bodnar, R.; Steinfink, H. *Inorg. Chem.* **1966**, *5*, 1469. (g) $ThSb_2$: Hulliger, F. *J. Less-Common Met.* **1968**, *16*, 113. (h) Sn and Ge: Donohue, J. *The Structures of the Elements*; Wiley: New York, 1974. (i) $SrAu_2$: See ref 31.

(10) (a) Row 6 parameters: Komiya, S.; Albright, T. A.; Hoffmann, R.; Kochi, J. K. *J. Am. Chem. Soc.* **1977**, *99*, 8440. (b) Underwood, D. J.; Hoffmann, R.; Tatsumi, K.; Nakamura, A.; Yamamoto, Y. *J. Am. Chem. Soc.* **1985**, *107*, 5968. (c) Row 4 parameters: Thorn, D. L.; Hoffmann, R. *Inorg. Chem.* **1978**, *17*, 126. (d) Row 5 parameters: Hughbanks, T.; Hoffmann, R.; Whangbo, M.-H.; Stewart, K. R.; Eisenstein, O.; Canadell, E. *J. Am. Chem. Soc.* **1982**, *104*, 3876.

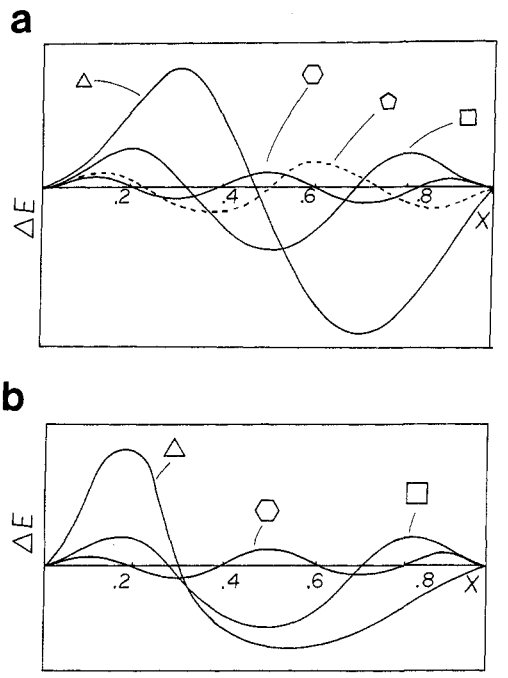

Figure 3. Qualitative energetic effect of different ring sizes as a function of electron count for (a) a uniform band and (b) an s and p band with a strong bonding tail. We plot in a (reproduced from ref 7) the difference in energy between a structure containing a single ring of bonded atoms and a structure with no rings at all. The following convention is used: if the value of the difference in energy is positive, then the structure with a ring is energetically more stable than the structure without a ring. The abscissa plots the fractional occupancy of the band in question. Thus, the three-membered ring structure is most stable for all low band fillings up to slightly less than the half-filled band.

simple crystal structures rarely (FeS_2 is an exception) contain five-membered rings. We therefore remove this curve from Figure 3b. Finally, it should be recalled that bond angles are a fourth- and fifth-moment effect. They too play a vital role in both crystal structures and Hückel calculations.

Second-Moment Equality

In order to compare these crystal structure types via a Hückel calculation, however, we need to develop a method to compare the six-coordinate $CuMg_2$, the four-coordinate MgAgAs, and the three-coordinate AlB_2 structure types. In order for two structure types to have the property that at one electron count one of the structures is favored while at another electron count the other is favored, it is necessary for the two structures to have approximately equal second moments. One technique that appears to give reliable results is to require for different structure types that

$$\sum_{\alpha,\beta,i,j} (S_{\alpha_i\beta_j})^2 = \text{constant} \qquad (1)$$

where α_i and β_j are orbitals, respectively, located on two atoms, α and β, that are bonded to each other, and $S_{\alpha_i\beta_j}$ is the overlap integral between them. As the expression (1) is proportional to the variance in the Hückel DOS, this procedure will lead to approximate equality of the two structure types' second moment.[7] In practice, therefore, one would first define the true coordination polyhedra in which the atoms sit, then one calculates the $\sum(S_{\alpha_i\beta_j})^2$, and finally one adjusts the a, b, and c unit cell parameters uniformly in such a way so as to make expression 1 true. A uniform change in the a, b, and c parameters leaves bond angles unchanged.

In Table II, we list the shortest interatomic distances. It may be seen that the above procedure is hampered by the presence of interatomic distances that are on the border between the weakly bonding and nonbonding regimes. In this paper, we adopt therefore a simpler condition in comparing structural energies. We sum that overlaps over all atom pairs (in practice, we truncate the sum at 10 Å). It will be seen that this technique gives quite reliable results in all but one case. In the one exception (that of

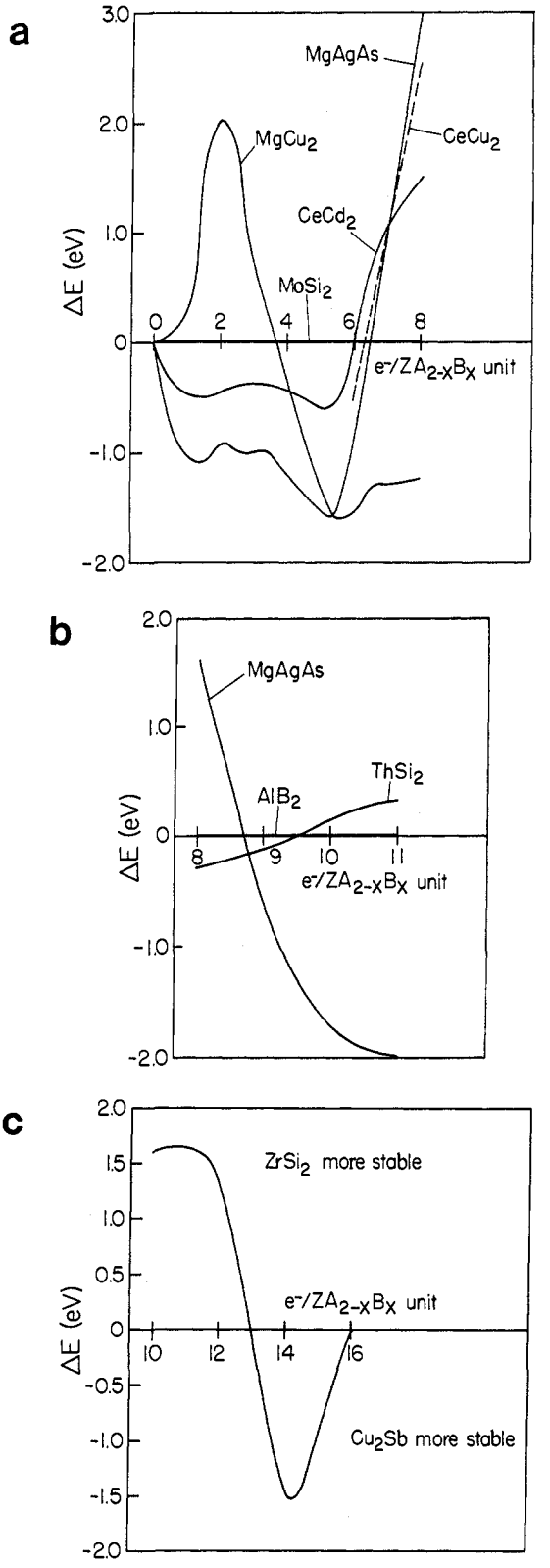

Figure 4. (a) Comparison of the energies of the $MgCu_2$, $MoSi_2$, $CeCd_2$, $CeCu_2$, and MgAgAs structure types. The curves plotted are the difference in energy between a given structure type and the $MoSi_2$ structure type. The conventions stated in the caption of Figures 1 and 3 are used. Energy is given in electronvolts per main-group atom. Note that at 7 $e^-/ZA_{2-x}B_x$ unit the $CeCd_2$, $CeCu_2$, and MgAgAs types are all equally favored. Calculational details are given in the Appendix. (b) Comparison of the energies of the MgAgAs, AlB_2, and $ThSi_2$ structure types. Difference in energy between a given structure type and the AlB_2 structure type is plotted. See the Appendix for calculational details. (c) Difference in energy between the $ZrSi_2$ and Cu_2Sb types. Positive values imply that the $ZrSi_2$ type is energetically more stable. See the Appendix for calculational details.

Table II. Selected Interatomic Distances for Representative Compounds

compd	struct type	interatomic distances (Å)	
$NaAu_2$	$MgCu_2$	Au–Au	2.76 (6x)
$GdAu_2$	$MoSi_2$	Au–Au	2.85 (1x)
			3.12 (4x)
			3.72 (4x)
$CeCd_2$	$CeCd_2$	Cd–Cd	2.98 (3x)
			3.45 (2x)
$SrAu_2$	$CeCu_2$	Au–Au	2.78 (3x)
			2.85 (1x)
Sn	diamond (MgAgAs)	Sn–Sn	2.81 (4x)
Ge	diamond (MgAsAs)	Ge–Ge	2.45 (4x)
$PrGa_2$	AlB_2	Ga–Ga	2.47 (3x)
$NdGe_2$	$ThSi_2$	Ge–Ge	2.36 (2x)
			2.45 (1x)
$ZrGe_2$	$ZrSi_2$	Ge(1)–Ge(1)	2.67 (4x)
		–Ge(2)	3.42 (2x)
		–Ge(2)	3.43 (2x)
		Ge(2)–Ge(2)	2.58 (2x)
		–Ge(1)	3.42 (2x)
		–Ge(1)	3.43 (2x)
$YbSb_2$	$ZrSi_2$	Sb(1)–Sb(1)	3.08 (4x)
		–Sb(2)	3.72 (2x)
		–Sb(2)	3.93 (2x)
		Sb(2)–Sb(2)	2.96 (2x)
		–Sb(1)	3.72 (2x)
		–Sb(1)	3.93 (2x)
$ThSb_2$	Cu_2Sb	Sb(1)–Sb(1)	3.08 (4x)
		–Sb(2)	3.98 (4x)
		Sb(2)–Sb(1)	3.98 (8x)

$ThSi_2$ compared to $ZrSi_2$), the final answer depends on whether very long interatomic distances are included in the calculation or not. (We discuss this in the following text).

Results of Band Calculations

In Figure 4, we show the energies found by Hückel calculations using the above method. Calculational parameters are given in the Appendix. We show in Figure 4a a comparison of the $MgCu_2$, $MoSi_2$, $CeCd_2$, $CeCu_2$, and MgAgAs structure types, in Figure 4b a comparison of the MgAgAs, AlB_2, and $ThSi_2$ types, and in Figure 4c a comparison of the $ZrSi_2$ and Cu_2Sb types. As low-electron-count Cu_2Sb is structurally quite similar to the $MoSi_2$ type, we do not perform a separate calculation for it. Similarly, MgAgAs and $CaIn_2$ correspond to, respectively, cubic and hexagonal diamond. They are structurally very similar, and we calculate only the cubic form. In Table I, we summarize and compare our theoretical model and the actual experimental results. It may be seen that the agreement is very good.

$ThSi_2$ vs $ZrSi_2$

A comparison of the $ThSi_2$ and $ZrSi_2$ structure types, however, does present some complications. We discuss here the origin of these complications. As may be seen in Figure 2, the $ZrSi_2$ structure is composed of two noninterconnected types of networks of bonded atoms. There is a square lattice and a zigzag chain of bonded atoms. The distance between the two is large (in $ZrSi_2$, the smallest interatomic distance between the square lattice and the chain is 3.40 Å). In Figure 5, we show a calculation comparing the energy between $ThSi_2$ and $ZrSi_2$ where the interaction between the two separate pieces of the $ZrSi_2$ structure is ignored. It may be seen that agreement between theory and experiment is excellent. However, we also show in Figure 5 a calculation where the interaction between the separate pieces is included. Although we may know chemically that the effect of such an interaction is quite small, the Hückel results do not bear this out. The problem appears to be that the Hückel theory does not properly weigh in the effect of interatomic interactions that are slightly greater than the distance for weak intraatomic bonds. We have discussed one method of handling this difficult situation in the earlier section Second-Moment Equality.

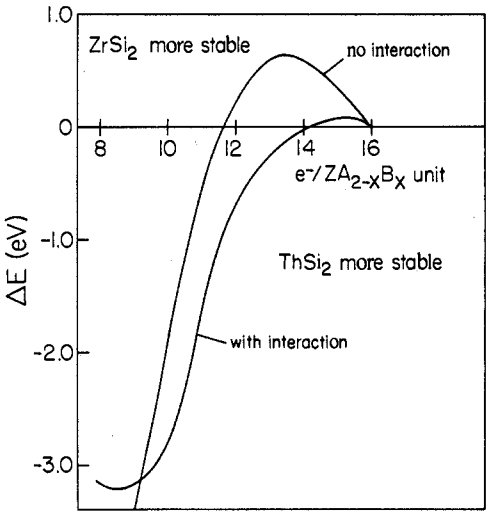

Figure 5. Difference in energy between the $ThSi_2$ type and the $ZrSi_2$ type. In the calculation marked "no interaction", the interaction between the square lattice and the zigzag chain of the $ZrSi_2$ type has been set equal to zero. The "with interaction" curve includes the effect of the square lattice to zigzag chain overlap. See Figure 4 caption for the conventions used and the Appendix for calculational details.

Finally, it should be remembered that we are studying here the role of only the electron count in determining structure type. Electron count, however, is only one of several well-known parameters. In a more powerful theory,[11] both size effects and the effect of differing electronegativities between the A and B atoms must also be included. Indeed, it is because we have not included these important factors that we have limited this study to the major structure types. By studying the aggregate collection of phases, we tend to statistically lessen the effects of other variables.

Acknowledgment. I thank Dr. Ludger Terbüchte, Scott Carter, and Min Lin for their helpful discussions and the Petroleum Research Fund, administered by the American Chemical Society, and the Rackham Graduate School for partial support of this research. The program used in our calculations is a modified version of the band program written at Cornell University by Roald Hoffmann, M.-H. Whangbo, T. Hughbanks, S. Wijeyesekera, M. Kertesz, C. N. Wilker, and C. Zheng. I also thank Dr. G. Miller for his irreducible-wedge k-space programs.

Appendix

The crystal structures of $NaAu_2$ ($MgCu_2$ structure type (st)), $GdAu_2$ ($MoSi_2$ st), $CeCd_2$ ($CeCd_2$ st), $SrAu_2$ ($CeCu_2$ st), and Sn (the diamond anion net of MgAgAs st) were used in the calculations of Figure 4a.[9] The parameters used were a combination of literature values for Au and Hg atoms:[10] $H_{ii}(6s) = -13.68$ eV, $H_{ii}(6p) = -8.46$ eV, $\zeta(6s) = 2.60$, and $\zeta(6p) = 2.58$. The atomic densities were scaled so that all crystal structures had the same second moment as that for the experimentally observed $GdAu_2$ phase. For Figures 4b and 5, the crystal structures of $NdGe_2$ ($ThSi_2$ st), $PrGa_2$ (AlB_2 st), Ge (diamond anion net of MgAgAs st), and $ZrGe_2$ ($ZrSi_2$ st) were used.[9] All atomic densities were adjusted to the $PrGa_2$ atomic density. Parameters for Ge[10] were $H_{ii}(4s) = -16.0$ eV, $H_{ii}(4p) = -9.0$ eV, $\zeta(4s) = 2.16$, and $\zeta(4p) = 1.85$. In Figure 4c, the crystal structures of $YbSb_2$ ($ZrSi_2$ st) and $ThSb_2$ (Cu_2Sb st) were used.[9] Hückel parameters[10] were $H_{ii}(5s) = -18.8$ eV, $H_{ii}(sp) = -11.7$ eV, $\zeta(5s) = 2.32$, and $\zeta(5p) = 2.00$. For face-centered cubic cells a 165 k-point mesh of the irreducible wedge was used, for tetragonal cells a 126 k-point mesh was used, for hexagonal or trigonal cells a 252 k-point mesh was used, and for orthorhombic cells a 27 k-point mesh was used.

(11) Villars, P. *J. Less-Common Metals* **1984**, *99*, 33.